Characterization of karst conduits by tracer tests for an artificial recharge scheme

Xinyu Cen[1] · Mo Xu[1] · Jihong Qi[1] · Qiang Zhang[1] · Haoxin Shi[1]

Abstract

Challenged by rapidly changing climate in combination with an increase in anthropogenic pressures, karst groundwater resources in the Old Town of Lijiang (OTLJ), SW China, are diminishing. Higher frequency and longer duration of dried-up periods have been observed at the Heilongtan Park (HP) Springs in recent years. Thus, there is an urgent need for an artificial recharge scheme, aimed at replenishing groundwater in the aquifer and increasing the outflow of the springs to ensure effective water resources management. Evaluation of the scheme feasibility, prior to its implementation, is important. In this study, tracer tests were conducted between the recharge area and receiving springs in order to gain insight into the transport mechanisms of karst groundwater and the structural characteristics of the aquifer. Multiple underground flow paths, exhibiting high conductivity between the recharge area and HP Springs, were revealed by the interpretation of tracer breakthrough curves. Three springs considered as the leakages of the scheme were identified. Moreover, the outflow of springs at HP and OTLJ were predicted to be increased by the artificially recharged water after 9.2 and 12.5 days, respectively. Quantitative analysis of tracer recoveries demonstrates that the springs to be recharged and the springs considered as leakages, respectively, share 45 and 55% of the increased outflow. The feasibility of the scheme has been confirmed by the tracer tests. This report provides references for the evaluation of artificial groundwater recharge and protection strategies, particularly in large and poorly investigated karst spring fields.

Keywords Karst · Tracer tests · Artificial recharge · Spring protection · China

Introduction

Karst regions cover 7–12% of the global land area, and almost a quarter of the world population is wholly or partially dependent upon drinking water derived from karst aquifers (Hartmann et al. (2014). Due to relatively small watershed size, the absence of a continuous supply of surface water, and increasing water consumption caused by population growth, karst groundwater is likely to become more prone to the adverse impacts of climate change (Klaas et al. 2020; Ostad-Ali-Askari et al. 2020; Sivelle et al. 2021). The projected reduction in water resources will challenge the

manufacturing industries, agriculture and fisheries, as well as people's daily lives all over the world (Goel and Kumar 2005; Nerantzaki and Nikolaidis 2020; Sun et al. 2017; Yin et al. 2020). Moreover, karst groundwater is associated with valuable landscape resources, and water scarcity and droughts can seriously damage the scenery associated with tourist attractions (Jiang et al. 2020; Luo et al. 2020; Ostad-Ali-Askari et al. 2017).

The Old Town of Lijiang (OTLJ) in Yunnan province, SW China, is listed as a World Heritage (Cultural) site by UNESCO for its incredible historical and cultural values. Located in the north of OTLJ, Heilongtan Park (HP) is known for its springs and pools, and it also serves as the water source of the OTLJ. However, due to insufficient precipitation and increasing extraction of groundwater in OTLJ, springs in HP have suffered from frequent drying up since 1960 (Han et al. 2019; Kang et al. 2013; Zeng et al. 2013). Between Jan. 2012 and Sept. 2014, HP Springs ceased flowing for approximately 956 days. Besides this, the frequency of drying up has increased from once every 20 years to once every 5 years since

✉ Mo Xu
xm@cdut.edu.cn

[1] State Key Laboratory of Geohazard Prevention and Geoenvironment Protection, Chengdu University of Technology, No. 1, Rd.3, Erxianqiao East, Chengdu 610059, China

1960. Consequently, the outflow of the springs in OTLJ has been decreasing in recent years; therefore, a series of actions are needed to preserve springs in HP and OTLJ.

Due to the rapidly changing climate and overexploitation of karst groundwater, the occurrences of attenuation and drying-up of karst springs are increasingly recorded globally (Hao et al. 2009; Schrader et al. 2014; Sivelle et al. 2021). To deal with these predicaments, regulation of groundwater extraction has been proposed and conducted (Al-Assa'd and Abdulla 2010; Kang et al. 2011); however, it is hard to meet expectations particularly in the areas exhibiting decreasing precipitation. Accordingly, managed aquifer recharge is considered as a promising sustainable technique for maintaining perennial outflow of karst springs and for enabling significant storage within the aquifers (Daher et al. 2011; Kang et al. 2011). This technique involves transferring multisource water (stormwater, surface water, etc.) into the karst aquifer by well injection and natural infiltration (Al-Assa'd and Abdulla 2010; Dar et al. 2017; Stevanović 2015; Xanke et al. 2016; Zhang and Wang 2021). Although a few operations have been conducted, the structure of the karst aquifer and transportation processes of water during the transition from supplied water to the outflow springs often remain unrevealed. Moreover, evaluation methods for the feasibility of these schemes are still theoretical and numerically based, while the field experiments are expected to deliver more valuable information. In this study, an artificial recharge scheme aiming at improving groundwater storage in a karstic aquifer and thus increasing the discharge of springs is introduced. To evaluate the feasibility of this scheme, field tracer tests have been conducted for further understanding of the karst aquifer.

Karst aquifers are characterized by strong heterogeneity and anisotropy, leading to complex system behavior (Knoll and Scheytt 2018). Artificial tracer tests have been widely utilized for determining the structures which cannot be explored directly by researchers in karst systems (Dewaide et al. 2018; Goldscheider 2008; Knoll and Scheytt 2018). The flow path geometry and number of major karst conduits have been successfully deduced from tracer tests (Long et al. 2008; Luhmann et al. 2012). The primary results of quantitative tracer tests are breakthrough curves (BTCs), i.e. the discrete or continuous series of concentration-time data (Goldscheider et al. 2008). Transport modeling of the BTCs is not only allowing considerable insight into groundwater flow and drainage networks, but also making it possible to predict travel times and transport characterization in the system (Morales et al. 2007; Ostad-Ali-Askari et al. 2019). BTCs are also of great value for the calibration of physically based groundwater flow models (Schilling et al. 2019). Oehlmann et al. (2015) utilized peak arrival times of BTCs for calibration of a karst system and therefore strongly reduced the ambiguity of karst aquifer models. Accordingly, transport modeling of the BTCs is considered as the key to deciphering the structural

properties and flow mechanism of the karst aquifer in this case.

In the following sections of this report, a short description of the study area and dried-up springs are first given, and then the artificial recharge scheme is introduced. To evaluate this scheme, artificial tracer tests are performed and the experimental BTCs are analyzed. Moreover, tracer recoveries, the conceptual model of karst conduits, and karst aquifer parameters are discussed. Finally, the article discusses the implication of tracer tests for the evaluation of an artificial recharge scheme in a karst spring field.

Methods and materials

### Drying-up of the Heilongtan Park Springs and the artificial recharge scheme

According to the local historical records, the earliest record of the drying-up of HP Springs can be dated back to the Qing Dynasty (1736) (Anonymous, *Lijiang Naxi Autonomous County Annals, 1997*). Since then, the drying-up of the springs has been repeatedly mentioned in the historical materials. The dried-up periods of HP Springs have been monitored by the Lijiang Hydrological Bureau since 1990 and the records are listed in Table 1. In addition, average monthly precipitation from four rain-gauge stations within the study area, discharge of the HP springs, and groundwater level measurements from the observation well are collected and shown in Fig. 1. The locations of the four rain-gauge stations and the observation well are shown in Fig. 2a.

Strong seasonal variation and significant correlation among precipitation, discharge, and groundwater level measurements can be observed in Fig. 1. In the period with abundant rainfall (1990–1991 and 1998–2002), discharge of HP Springs and groundwater level are high, ranging from 1 to 4 m^3/s and 2,407 to 2,413 m respectively. While in the years with insufficient precipitation (1992–1997 and 2003–2011), groundwater level drops by 2–5 m, and discharge of HP Springs decreases by 1–2 m^3/s, leading to frequent drying up of HP Springs, indicated by the red circles in Fig. 1.

Table 1 Recorded dried-up periods of HP Springs since 1990

Period of drying-up	Days of dry-up
26 Jun. to 9 Aug. 1993	45
10 May to 31 Jul. 1995	82
14 May to 24 Jul. 2006	71
19 Mar. to 25 Jul. 2007	128
14 Jun. to 22 Aug. 2010	69
23 Jan. 2012 to 5 Sept. 2014	956

Fig. 1 a Monthly mean discharge of HP springs and groundwater level from Jan. 1990 to Dec. 2011. Dried-up events are highlighted by the red circles. The groundwater level has been normalized by the reference value of 2,405 m for a better display of the trend. **b** Distribution of monthly mean rainfall from four rain-gauge stations in every year from 1990 to 2011. Medians (orange lines) and outliers (black squares) of rainfall are also displayed
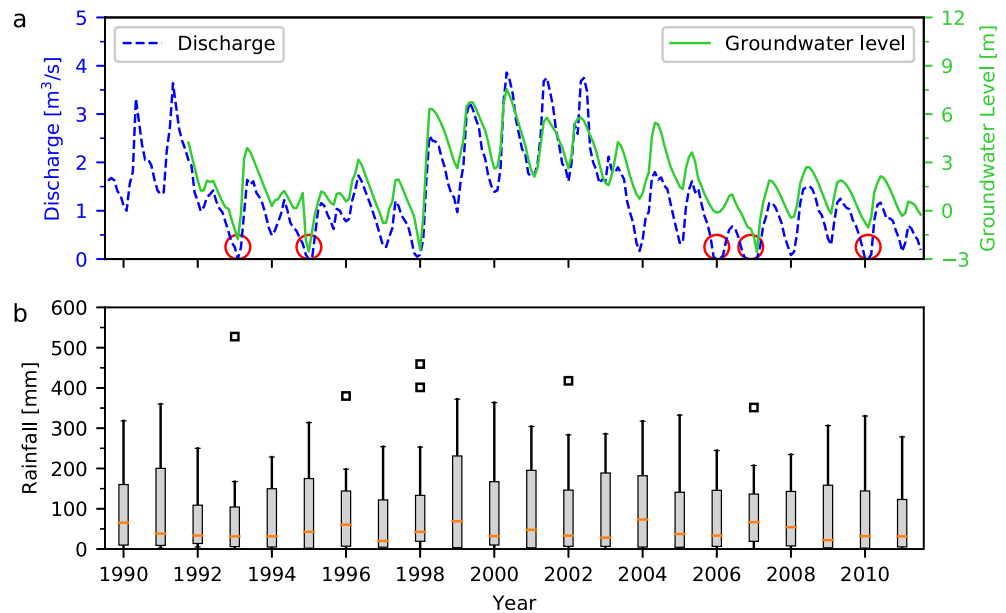
According to the survey of water consumption in Lijiang City, the amount of exploitation of karst groundwater was very low before 2005, yet two periods of drying up at HP Springs were recorded, in 1993 and 1995. The level of exploitation has increased significantly due to the development of local industry and tourism since 2006, and has led to a higher frequency and longer duration of drying up from 2006 to 2011, although the precipitation during this period was almost the same as that recorded before 1998. Thus, it can be deduced that the drying-up of HP Springs is fundamentally driven by insufficient precipitation and, at the same time, greatly influenced by overexploitation of the groundwater resource. This finding is consistent with the previous studies conducted by Kang et al. (2013) and Zeng et al. (2013). By Oct. 2018, measurements from observation wells show that the groundwater is close to being restored to the level before 2005, owing to efforts that have been undertaken to regulate the overexploitation since 2017. However, a managed aquifer recharge scheme for restoring and preserving the groundwater resources of HP and OTLJ is considered as the optimal solution. Taking surface water, ecology, and especially the geological and hydrogeological conditions into account, an artificial recharge scheme is proposed. This scheme consists of constructing a reservoir in a karst depression 17 km north of HP, transferring water from nearby rivers into the reservoir through ditches, and finally recharging springs in HP and OTLJ by replenishing the karst aquifer. In this context, field tracer tests were chosen to characterize the karst aquifer and evaluate the feasibility of this artificial recharge scheme. It should be noted that the construction and water-transfer processes are not in the scope of this report.

Study area

Located in the northwest of Yunnan Province, SW China, the Old Town of Lijiang is listed as a World Heritage (Cultural) site by UNESCO for its incredible historical and cultural values, see Fig. 2a. With a population of more than 1.2 million, the study area is characterized by a monsoon climate with typical wet and dry seasons. Annual precipitation in the catchment averages 957.2 mm, predominantly occurring from June to September (Zeng et al. 2015). The annual average temperature is 16.3 °C in Lijiang (Qi et al. 2018).

Surrounded by a variety of outcropping strata including Triassic limestone (T), Permian basalt (P), Eocene calcibreccia (E) and Quaternary sediments (Q), the study area shows elevation ranging from 2,396 to 3,500 m above sea level (asl). Along the eastern foothills, an impermeable fault (F1) striking approximately N–S presents a hydrogeological boundary and it also separates the Triassic limestone and Permian basalt. Triassic carbonate aquifers are found predominantly cropping out in the mountainous areas, offering favorable paths for karst groundwater. The aquifers are covered by Eocene calcibreccia and Quaternary sediments in the south and Jiuzihai karst depression, respectively (Fig. 2a).

As suggested by Fig. 2b, being the main aquifers, the middle Triassic limestone strata presents valuable landscape and supplies domestic water for HP and OTLJ. With an area of more than 8.2 km^2 as well as favorable precipitation confluence conditions composed by sinkholes and the surrounding higher elevations, Jiuzihai karst depression forms the main recharge area of this spring field. Aquifers are rapidly recharged by surface water coming from precipitation (Pu et al. 2013). Groundwater is generally flowing from northeast
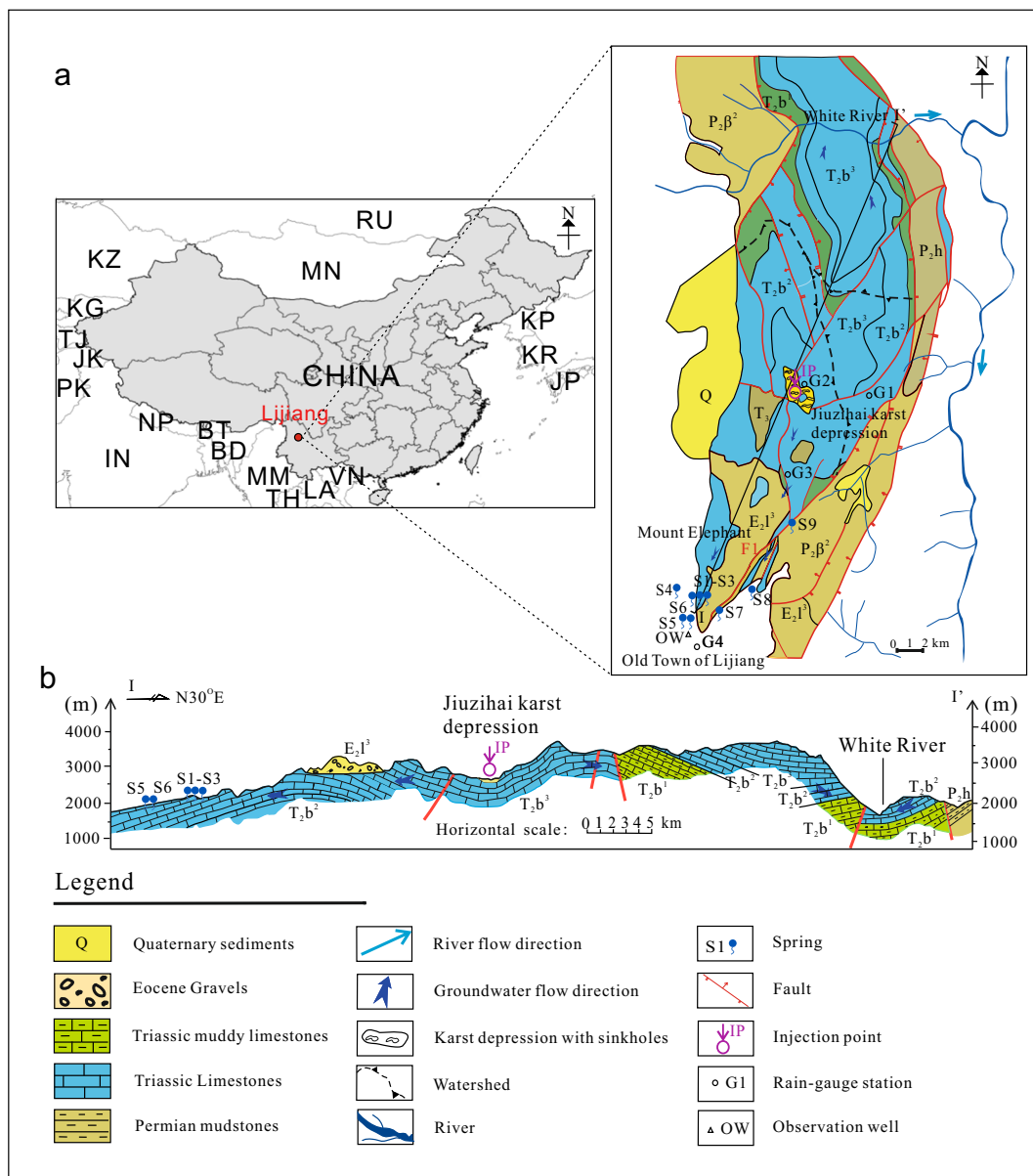
Fig. 2 **a** Geographical situation and hydrogeological map of study area and **b** hydrogeological cross section of the study area

to southwest and discharging through springs situated at the F1 fault zones as well as contact between carbonate exposures and impervious formations including the Permian basalt and Quaternary sediments.

Tracer tests

In 2014, multi-tracer tests were conducted from November to December. Uranine (3 kg) and potassium iodide (KI) powder (400 kg) were dissolved in 300 m^3 water and injected quasi-instantaneously (within 2 h) into the sinkhole of Jiuzihai karst depression (Fig. 2). A large volume of water (1×10^6 m^3) was subsequently introduced for the next 24 h in order to flush the tracers into the aquifer. Groundwater samples were taken at nine

springs. In addition to the three springs in HP (S1, S2, and S3) and three springs in OTLJ (S5, S6, and S7), Clear Spring (S4) and Fault Springs (S8 and S9) which were serving as the main outlets of the karst system, were also selected as the receiving points for determining the potential leakage of the scheme (Fig. 2a). Before the tests, standard samples from every receiving point were collected and measured for use in calibration. At every receiving point, water samples were first taken once a day and then the sampling interval gradually decreased to every 2 h with the increase of concentration. The frequent sampling lasted until the peaks passed, and then the interval gradually increased for the next few days. Sampling campaigns were conducted for 1 month, with a total of 934 water samples collected. Samples were analyzed in the

field, using a DR6000 UV spectrometer. During the experiment, the springs' discharge was recorded along with the sampling, which suggested an almost constant rate at each receiving point. There were no rainfall events in the study area according to the field observations and meteorological data provided by the regional authorities.

Curve fitting

All observed breakthrough curves were fitted with the multidispersion model (MDM) and the two-region nonequilibrium (2RNE) model using the software CXTFIT (Toride 1995). Theoretically, MDM could be interpreted as a superposition of the individual flow paths characterized by the conventional advection-dispersion model (ADM; Field and Leij 2012):

$$\frac{\partial C}{\partial t} = D\frac{\partial^2 C}{\partial x^2} - v_m\frac{\partial C}{\partial x} \tag{1}$$

where C is the aqueous concentration at time t [M/L^3], D is the longitudinal dispersion [L^2/T], v_m is the mean flow velocity [L/T] and x is the length of the flow path [L]. The basic assumption of MDM is that each flow path is characterized by different flow velocities and dispersivities (or dispersion parameters). It is assumed (1) that the mass of tracer injected is divided into several flow paths proportional to the volumetric flow rates along those paths and (2) that there are no interactions between the flow paths (Leibundgut et al. 2009). Therefore, the outlet of the karst system, in this case the spring, can be regarded as a place where the tracer distributed in each flow path finally converges. The MDM was initially developed for tracer transport in heterogeneous multilayered porous media but can also be applied to karst aquifers with multiple flow paths (Kübeck et al. 2013; Małoszewski et al. 2006; Maloszewski and Zuber 1992).

In ADM, the mean flow velocity (v_m) and longitudinal dispersion coefficient (D) were firstly estimated by fitting the modeled BTCs to observed values. Advection can be expressed as mean v_m. Dispersion can be described by the D or the longitudinal dispersivity $\alpha = D/v$ (Goeppert and Goldscheider 2019). The general advection–dispersion equation (Eq. 1) is solved analytically by assuming homogeneous profiles, a uniform and unidirectional flow field that is constant in time and space, and constant flow parameters (van Genuchten et al. 2012). A stepwise determination of the transport parameters needs to be realized for modeling multiple peaks in CXTFIT (Goeppert and Goldscheider 2019). The earliest peak of the BTC should be fitted firstly for the determination of v_m and D, then subtracted. The residual concentrations are used for further fitting until the last peak is completed.

For relatively simple right-skewed curves, the 2RNE model has been confirmed to be effective by numerous studies (Barberá et al. 2017; Field and Pinsky 2000; Lauber et al. 2014). By accounting for mobile and immobile fluid phases, this approach assumes that the persistent skewness of curves is attributed to immobile fluid regions. Since the 2RNE model further accounts for the two regions and the exchange process, the advection-dispersion equation has been extended by two parameters, a portioning coefficient β, and a mass transfer coefficient ω. Thus, a total of four parameters (v_m, D, β, and ω) need to be fitted simultaneously (Lauber et al. 2014).

Results and discussion

General results of tracer tests

A set of 12 parameters (see abbreviations and descriptions in Table 2) were considered for the analysis of the BTCs. These variables include tracer mass, time of travel, time difference,

Table 2 Description of the parameters

Notation	Definition	Unit
m_0	Injected tracer mass	[M]
m_R	Recovered tracer mass	[M]
R	Tracer recovery	[−]
t_{le}	Time-of-travel of the leading edge	[T]
t_p	Time-of-travel of the peak concentration	[T]
v_{le}	Flow velocity considering the time of leading edge as reference	[L T^{-1}]
v_p	Flow velocity considering the time of peak concentration as reference	[L T^{-1}]
C_p	Maximum concentration of peak	[M L^{-3}]
∇h	Difference in level between injection point and spring	[L]
x	Radial distance between injection point and spring	[L]
Q	Discharge during the tracer experiment	[L^3 T^{-1}]
I	Groundwater hydraulic gradient	[−]

Table 3 Hydrogeological information and characteristic parameters for tracer tests in the study area

BTC	Tracer	m_0 [kg]	m_R [kg]	R [%]	t_{le} [h]	t_{p1} [h]	t_{p2} [h]	t_{p3} [h]	v_{le} [m/h]	v_{p1} [m/h]	v_{p2} [m/h]	v_{p3} [m/h]	C_{p1} [µg/L]	C_{p2} [µg/L]	C_{p3} [µg/L]	∇h [m]	x [km]	Q [L/s]	I [%]
BTC1	Γ^-	400	0.01	0.003	186	222	332	448	80.65	67.57	45.18	33.48	16.86	47.43	52.36	420	15	0.5	2.6
	Uranine	3	0.002	0.67	216	222	291	432	69.44	67.57	51.55	34.72	5.08	18.56	23.05				
BTC2	Γ^-	400	0.574	0.144	189	220	332	422	79.37	68.18	45.18	35.55	25.2	41.87	44.65	420	15	33.5	2.6
	Uranine	3	0.058	1.93	220	222	308	404	68.18	67.57	48.7	37.13	4.26	14.07	9.58				
BTC3	Γ^-	400	0.102	0.026	186	222	340	428	80.65	67.57	44.12	35.05	30.75	36.96	61.33	420	15	5.5	2.6
	Uranine	3	0.009	0.3	210	226	286	404	71.43	66.37	52.45	37.13	9.58	13.26	9.58				
BTC4	Γ^-	400	2.054	0.514	144	192	282	—	108.3	81.25	55.32	—	236.6	247.2	—	407	15.6	40	2.6
	Uranine	3	0.144	4.8	180	216	312	—	86.67	72.22	50	—	16.76	19.91	—				
BTC5	Γ^-	400	0.433	0.108	222	298	—	—	72.97	54.36	—	—	105	—	—	443	16.2	14.2	2.7
	Uranine	3	0.048	1.6	222	310	—	—	72.97	52.26	—	—	13.21	—	—				
BTC6	Γ^-	400	0.054	0.014	250	318	—	—	64.8	50.94	—	—	121.1	—	—	432	16.2	3.1	2.7
	Uranine	3	0.005	0.167	270	332	—	—	60	48.8	—	—	10.61	—	—				
BTC7	Γ^-	400	0.337	0.084	216	270	—	—	70.83	56.67	—	—	140.3	—	—	444	15.3	17.4	2.9
	Uranine	3	0.024	0.8	234	270	—	—	65.38	56.67	—	—	10.26	—	—				
BTC8	Γ^-	400	0.307	0.077	144	186	—	—	89.58	69.35	—	—	176.2	—	—	419	12.9	7	3.2
	Uranine	3	0.028	0.933	144	180	—	—	89.58	71.67	—	—	13.07	—	—				
BTC9	Γ^-	400	0.32	0.08	132	192	—	—	71.21	48.96	—	—	211.5	—	—	343	9.4	3.9	3.6
	Uranine	3	0.027	0.9	132	174	—	—	71.21	54.02	—	—	25.32	—	—				

tracer velocity, tracer concentration, geographical distance, and spring discharge. The tracer recovery rates (R) were calculated using the discharge (Q):

$$R = \frac{m_R}{m_0} = \frac{1}{m_0} \int_{t=0}^{\infty} Q \cdot C(t)dt \qquad (2)$$

where m_0 is the injected tracer mass and $C(t)$ is the aqueous concentration at time t (Field and Nash 1997).

As shown in Figs. 4 and 5, Γ^- and uranine were detected at all receiving points, confirming the connectivity between Jiuzihai karst depression and all springs. The observed BTCs of the two tracers received at each spring show similar morphology. The curves observed at HP Springs (S1, S2 and S3) and Clear Spring (S4) are triple-peaked and double-peaked respectively (Fig. 4), while the rest of the curves show a single peak (Fig. 5). Almost identical first detection times for two tracers were observed at S5 (222 h), S8 (144 h), and S9 (132 h), while Γ^- was generally first detected 20–30 h earlier than uranine at the remaining springs. For the HP Springs, the first peaks of two tracers were reached after 220 h, while the second peaks acquired from Γ^- were detected about 45 h earlier than that from uranine (Fig. 3; Table 3). The first peak of Γ^- was observed 192 h after injection at S4, which was 25 h earlier than uranine. Regarding the single-peaked curves obtained at OTLJ Springs (S5, S6, and S7), maximum concentrations of two tracers were measured after 300, 320, and 270 h, respectively. The average t_{p1} is about 180 h at Fault Springs (S8 and S9).

The concentrations of uranine were significantly lower than that of Γ^- at every receiving point due to the distinctive injected mass (Table 3). Among all springs, the lowest first peak concentrations (C_{p1}) of Γ^- were observed at HP Springs, with concentrations of 16.86, 25.2 and 30.75 µg/L. While the highest C_{p1} (236.6 µg/L) of Γ^- was measured at Clear Spring. The C_{p1} of 5.08, 4.26, 9.58 and 16.76 µg/L were recorded for uranine at those springs respectively. Relatively medium C_{p1} values were found at the OTLJ Springs, for which variations ranged from 105 to 140.3 µg/L and 10.26 to 13.21 µg/L for Γ^- and uranine, respectively. Generally higher C_{p1} of 176.2 to 211.5 µg/L (Γ^-) and 13.07 to 25.32 µg/L (uranine) were found at Fault Springs.

The flow velocity considering the time of the first peak (v_{p1}) at HP Springs was measured as approximately 68 m/h for both tracers (Fig. 3; Table 3). The highest v_{p1} (81.25 m/h) was calculated with Γ^- at S4, and the velocity of 72.22 m/h was derived from uranine. v_{p1} values of between 48.8 and 56.67 m/h were calculated with both tracers at OTLJ Springs. Regarding the Fault Springs, v_{p1} of S8 (69.35 and 71.67 m/h for Γ^- and uranine respectively) were noticeably higher than that of S9 (48.96 and 54.02 m/h respectively). Overall, the highest v_{p1} was observed at S4, followed by HP Springs, S8, OTLJ Springs and S9.

Fig. 3 Scatterplots of velocities and time: **a** results from I^- and **b** results from uranine. See Table 1 for definition of terms
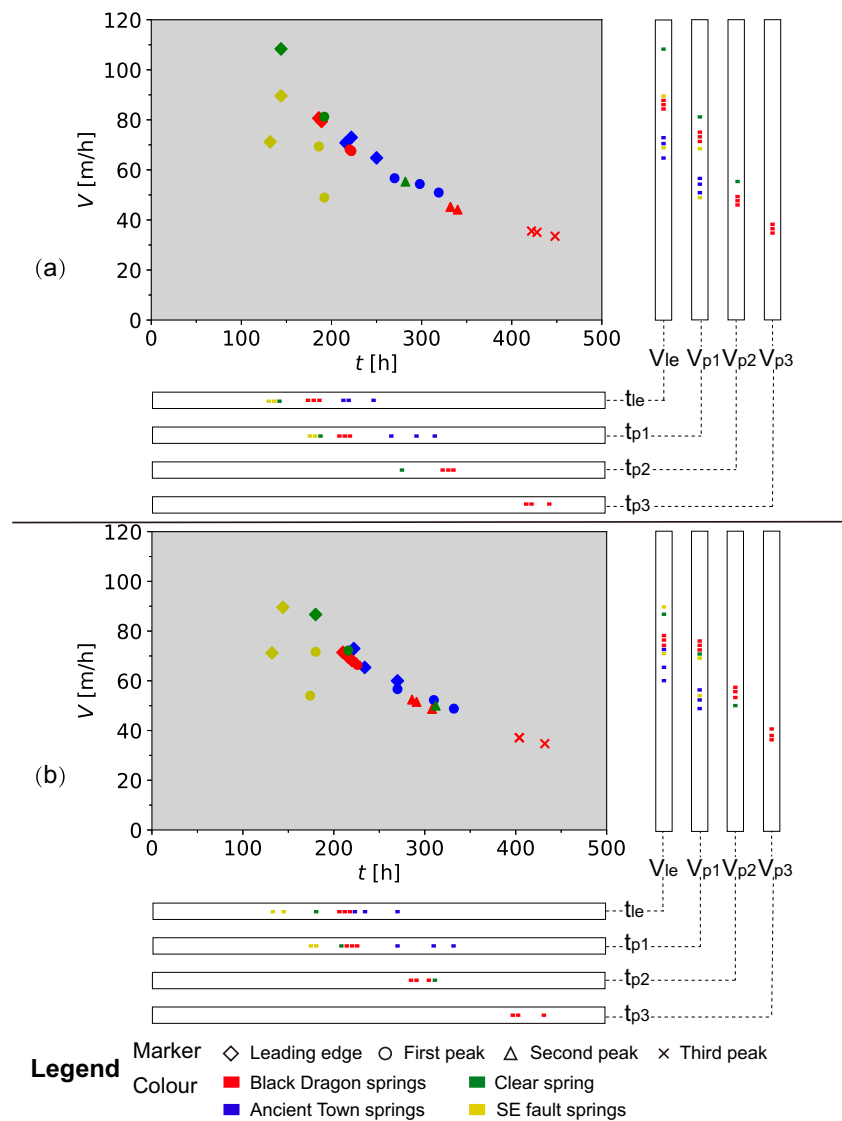
Multi-peaked BTCs and transport parameters of the MDM

Triple-peaked and double-peaked curves were acquired at HP Springs and Clear Spring, respectively (Fig. 4). Multi-peaked BTCs have always been considered as emblematic of anastomoses in the karst aquifer (Field and Leij 2012; Goldscheider 2008; Perrin and Luetscher 2008). Although other factors including precipitation events and injection mode of tracers may be responsible for multi-peaked BTCs as well (Brouyère et al. 2005), there were no precipitation events over the experiment period and the tracers were injected into the sinkhole within 2 h, which can be regarded as instantaneous release compared with the total test time of 600 h. Therefore, it can be inferred that (1) three major flow paths (FP) exist between Jiuzhai karst depression and HP Springs and, (2) two major flow paths exist between the depression and Clear Spring.

Regarding the HP Springs, almost identical mean flow velocities (v_m) derived from two tracers are recognized for every FP (Fig. 4a–f). It should be noted that the flow velocities derived from FP2 and FP3 are 1.5–2.5 times smaller than that from FP1. The highest v_m value (80.33 m/h) among all springs was modeled from the FP1 at Clear Spring, which is consistent with the v_{p1} (81.25 m/h) calculated from observation values. Generally, longitudinal dispersion (D) differs for two tracers (Fig. 6a,b): maximum and minimum values generated from I^- are 5,236 m²/h (S4) and 471.7 m²/h (S3), while those obtained from uranine are 1,562 m²/h (S4) and 221 m²/h (S3). It can be noted that Clear Spring exhibits significantly higher values of D than HP Springs, owing to the higher flow velocities. In addition, it can be inferred from Fig. 4 and Table 4 that the data acquired from I^- fits better with the MDM, and this is suggested by higher R^2 ranging from 0.951 to 0.975 compared with 0.88 to 0.974 derived from uranine.

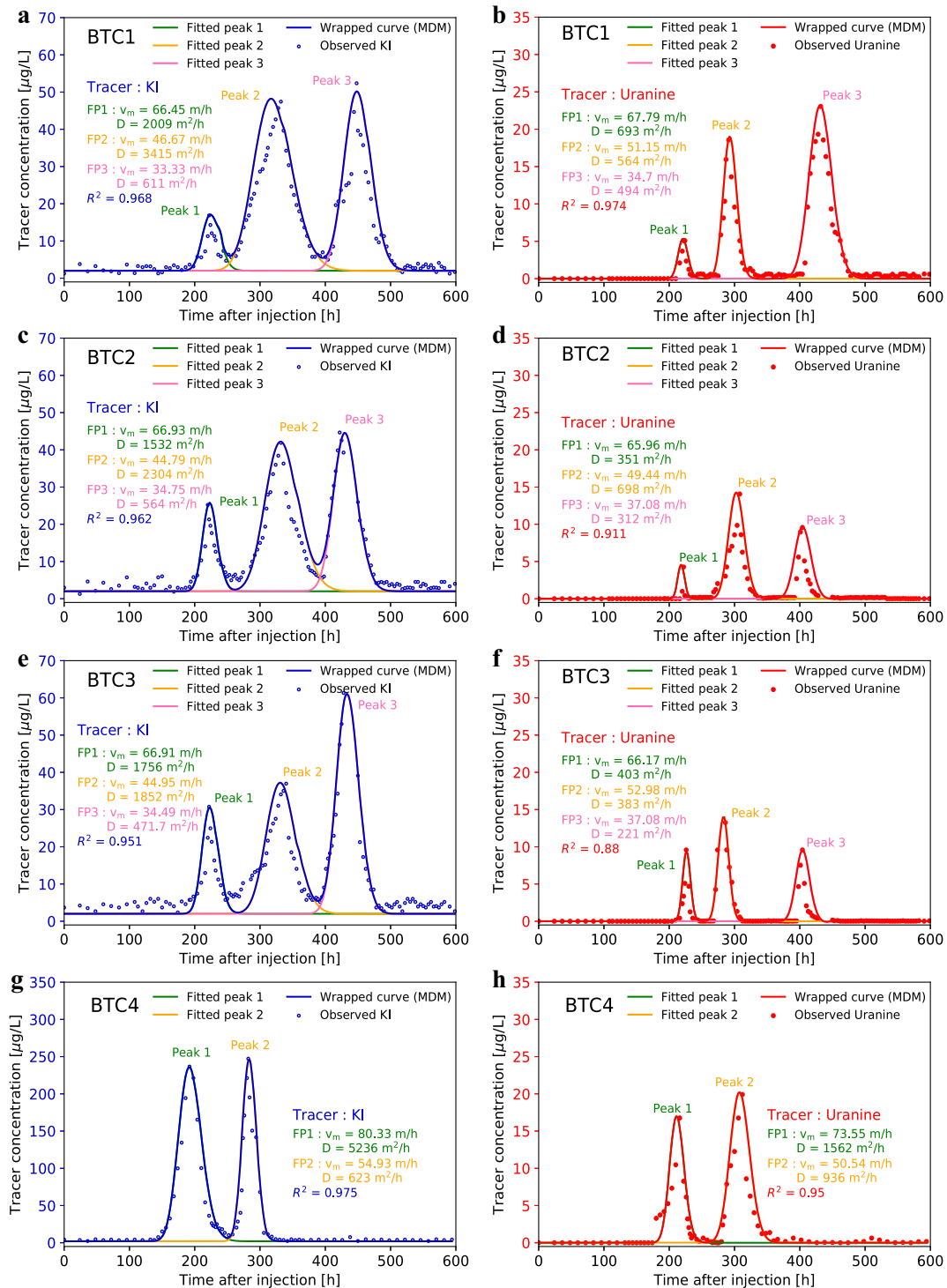**Fig. 4** **a**–**h** Transport simulation results of multipeaked breakthrough curves (BTCs) based on the application of MDM equations

Single-peaked BTCs and transport parameters of 2RNE model

All the BTCs resulting from the OTLJ Springs show a single and nearly symmetric peak (Fig. 5a–c), while asymmetric curves with persistent skewness are obtained from Fault Springs (Fig. 5d,e). The persistent skewness is commonly

attributed to immobile-flow regions that have been confirmed by numerous studies (Field and Leij 2012; Field and Pinsky 2000). In practical terms, dead-end passages, fissured matrix, storage of tracer in large cavities, as well as cave breakdown (roof collapse) are expected to have a major effect on solute transport, creating no-flow regions (Field and Pinsky 2000; Geyer et al. 2007; Goldscheider 2008; Li and Field 2014).

Table 4 Parameters of the multi-dispersion model (MDM) obtained from artificial tracer tests at springs S1–S4

Parameter			Springs and tracers							
			S1		S2		S3		S4	
			I$^-$	Uranine	I$^-$	Uranine	I$^-$	Uranine	I$^-$	Uranine
1st peak										
Mean flow velocity	v_m	[m/h]	66.45	67.79	66.93	65.96	66.91	66.17	80.33	73.55
Mean transit time (calc.)	t_m	[h]	225.74	221.26	224.1	227.4	224.17	226.68	194.2	212.1
Longitudinal dispersion	D	[m^2/h]	2009	693	1,532	351	1756	403	5236	1562
Dispersivity	α	[m]	27.65	9.35	20.93	4.87	24	5.57	65.18	21.24
2nd peak										
Mean flow velocity	v_m	[m/h]	46.67	51.15	44.79	49.44	44.95	52.98	54.93	50.54
Mean transit time (calc.)	t_m	[h]	321.38	293.28	334.9	303.37	333.67	283.1	284	308.67
Longitudinal dispersion	D	[m^2/h]	3,415	564	2,304	698	1,852	383	623	936
Dispersivity	α	[m]	66.92	10.09	47.05	12.91	37.68	6.61	11.34	18.52
3rd peak										
Mean flow velocity	v_m	[m/h]	33.33	34.7	34.75	37.08	34.49	37.08	–	–
Mean transit time (calc.)	t_m	[h]	450.05	432.26	431.69	404.54	434.9	404.51	–	–
Longitudinal dispersion	D	[m^2/h]	611	494	564	312	471.7	221	–	–
Dispersivity	α	[m]	16.77	13.02	14.85	7.7	12.51	5.45	–	–
Coeff. of determination	R^2	–	0.968	0.974	0.962	0.911	0.951	0.88	0.975	0.95

Thus, it can be inferred that (1) there is only one major flow path that exists between Jiuzihai karst depression and S5–S9, and (2) no-flow regions exist along the flow path between the depression and Fault Springs (S8 and S9).

The mean flow velocity (v_m) of 52.9 m/h was calculated at OTLJ Springs (Table 5). Although there is no noteworthy difference in v_m among the simulated results from the springs, the average dispersion (4,008 m^2/h) of S5 is significantly higher than that of S6 (1,285 m^2/h) and S7 (1,191.5 m^2/h; Fig. 6a,b). Regarding the Fault Springs, two parameters of S8 (v_m = 55.53 m/h, D = 2885.5 m^2/h) were markedly higher than those of S9 (v_m = 36.79 m/h, D = 1,472.5 m^2/h). The BTCs acquired from the OTLJ Springs deliver higher partition coefficients (0.8–0.95) than those from the Fault Springs (0.71–0.8), suggesting the higher contribution of the mobile-flow regions during transporting (Fig. 6c). In contrast, OTLJ Springs (0.005–0.09) yield lower transfer coefficients than the Fault Springs (0.4–1.23), implying less-intense solute exchange (Fig. 6d). The coefficients of determination (R^2) ranged from 0.933 to 0.989 suggesting a quite good fit; moreover, the coefficients fitted for I$^-$ (0.979–0.989) are generally higher than those for uranine (0.933–0.979). The rising and receding limbs of BTCs are both quite well fitted for the relatively symmetric curves obtained from OTLJ Springs, while the rising limbs are fitted much better than the receding limbs for the curves exhibiting persistent skewness obtained from Fault Springs (Fig. 5).

Tracer recoveries

In the field tests, salt (I$^-$) and fluorescence (uranine) were used as artificial tracers. Despite direct injection into the sinkhole, total tracer recoveries only reached 0.164 and 12.1% for I$^-$ and uranine, respectively (Table 3). This finding can be related to the following causes. Firstly, long tracing distance (up to 16.4 km without considering tortuosity) and large study area (approximately 150 km^2) may lead to high retention of tracers in the karst system. Secondly, considering the possibility of seasonal karst springs as well as the limitation of field investigation, it is very likely that some springs were not found and then missed monitoring during the tests. Finally, tracer may enter deep flow paths and the regional flow system according to the local and regional flow pattern in mountainous areas, as summarized by Tóth (1963).

It can be further noted that total recoveries of I$^-$ are almost two orders of magnitude lower than that of uranine. This difference in recoveries can be attributed to the different properties of tracers. Uranine is an ideal tracer with conservative properties, while care should be exercised about the potential conversion of iodine species under different geochemical conditions (Hu and Moran 2005; Leibundgut et al. 2009). Hu and Moran (2005) concluded that the conversion of iodide to iodate or elemental iodine under oxidizing conditions will confound the interpretation of a tracer study's results. Furthermore, iodate is more reactive and exhibits retarded
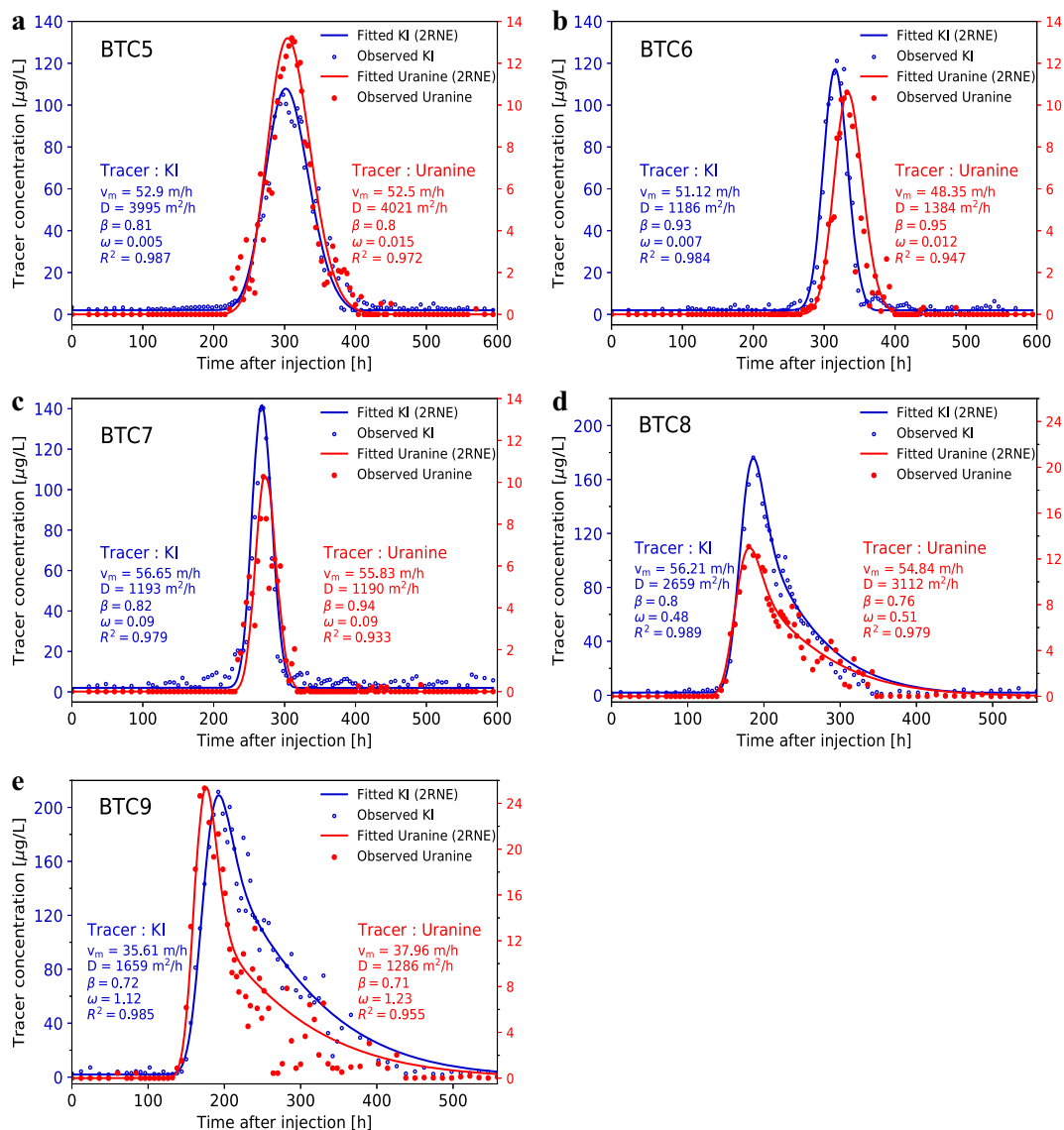
Fig. 5 Transport simulation results of single-peaked breakthrough curves (BTCs) based on the application of 2RNE equations

Table 5 Parameters of the two-region nonequilibrium (2RNE) model obtained from artificial tracer tests at springs S5–S9

Parameter			Springs and tracers									
			S5		S6		S7		S8		S9	
			Γ	Uranine	Γ	Uranine	Γ	Uranine	Γ	Uranine	Γ	Uranine
Mean flow velocity	v_m	[m/h]	52.9	52.5	51.12	48.35	56.65	55.83	56.21	54.84	35.61	37.96
Mean transit time (calc.)	t_m	[h]	306.24	308.57	316.9	335.06	270.08	274.05	229.5	235.23	263.97	247.63
Longitudinal dispersion	D	[m²/h]	3,995	4,021	1,186	1,384	1,193	1,190	2,659	3,112	1,659	1,286
Dispersivity	α	[m]	75.52	76.59	23.2	28.62	21.06	21.31	47.3	56.75	46.59	33.88
Partition coefficient	β	–	0.81	0.8	0.93	0.95	0.82	0.94	0.8	0.76	0.72	0.71
Mass transfer coefficient	ω	–	0.005	0.015	0.007	0.012	0.09	0.09	0.48	0.51	1.12	1.23
Coeff. of determination	R^2	–	0.987	0.972	0.984	0.947	0.979	0.933	0.989	0.979	0.985	0.955

Fig. 6 **a–b** Scatterplots between longitudinal dispersion (D) and mean flow Velocity (v_m) calculated from I^- and uranine respectively, using MDM and 2RNE models. **c–d** scatterplots among parameters obtained from 2RNE; results from I^- and uranine are marked by unfilled circles and filled circles, respectively
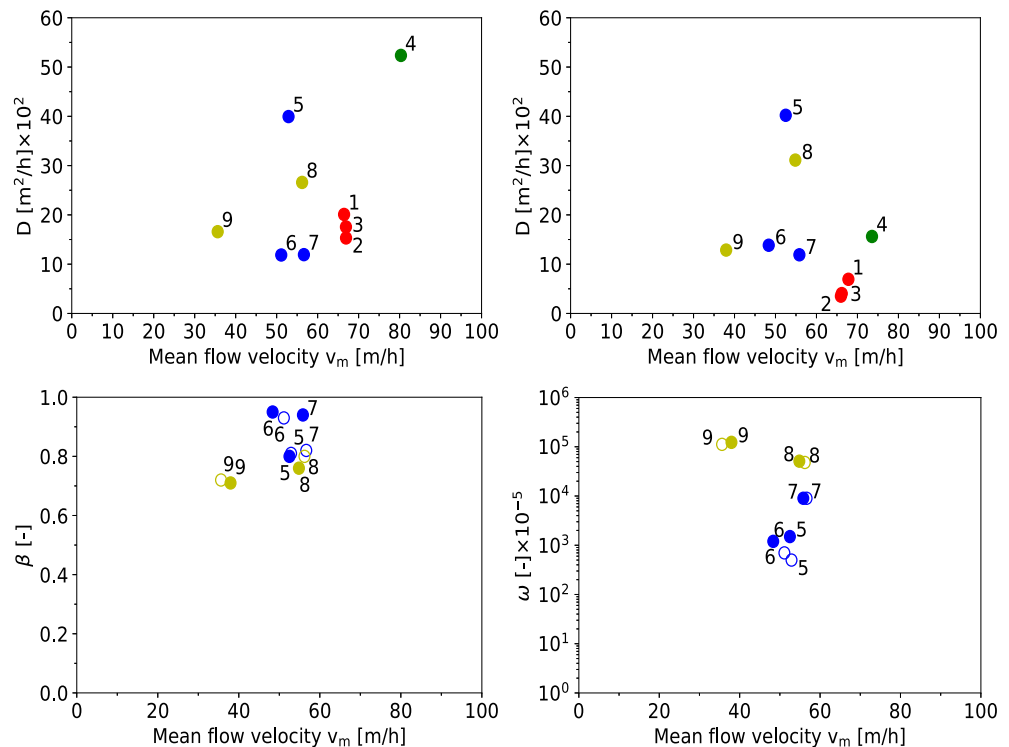
transport due to its interactions with clays and organic matter (Couture and Seitz 1983; Yoshida and Uchida 1992). According to the field survey, fractures filled with red clay are widely developed in the main aquifer (T_2b). The red clay provides favorable conditions for the oxidation of iodide anion and the reaction of iodate.

Conceptual model of karst conduit and karst aquifer parameters

According to the tracer tests, Jiuzihai karst depression and HP Springs are deduced to be connected by three major flow paths (Fig. 7). In addition, almost identical breakthrough curves were obtained at three springs in HP, suggesting these springs are individual outlets of the same drainage system. Different tracer recoveries are attributable to varying discharges, which occur possibly due to different pressure conditions and sizes of the outlets. The fast-flow component is associated with larger velocities and dispersions, indicating high advective and turbulent flow in the conduits, while the lower-flow component occurs due to the flow through well-drained fractures and fissures. There are two main branches of drainage between the depression and Clear Spring (Fig. 7). Several highest-value parameters and modeling results, including tracer concentrations, velocities, recoveries, discharge and dispersion coefficients, were acquired at Clear Spring (Tables 3 and 4). The highest value for dispersion, determined by I^- at S4, is 5,236 m^2/h for the first peak, which can be attributed to the effect of rapids in the drainage system. It should be noted that

the velocities and dispersion coefficients derived from S4 are noticeably higher than that from S1–S3 despite the identical value of hydraulic gradient being obtained. This implies that the underground pathway leading to Clear Spring is characterized by higher permeability than that to HP Springs. According to the relations between flow conditions and maximum tracer concentrations in the karst aquifer described by several studies (Goppert and Goldscheider 2008; Lauber and Goldscheider 2014; Pronk et al. 2007, 2009), it can be deduced that the highest maximum concentrations acquired at Clear Spring resulted from higher flow velocities. In addition, the highest discharge and concentrations among all observed results delivered the maximal tracer recoveries at Clear Spring.

There is only one major drainage from Jiuzihai karst depression to the OTLJ Springs (Fig. 7). Although the values of radical tracing distance (x) and hydraulic gradient (I) obtained from OTLJ Springs and HP Springs are similar, velocities calculated at S5–S7 were found to be about 20 m/h smaller than those at S1–S3. This indicates that the flow path between the depression and OTLJ Springs is featured with lower permeability compared with that between the depression and HP Springs. Results with the 2RNE model show a high percentage of karst water transferring within the mobile fluid region (80–95%), indicating highly heterogeneous and anisotropic flow paths. In contrast, a limited rate of exchange between the mobile-fluid and immobile (no flow) regions can be deduced according to the low mass transfer coefficients (0.005–0.09), suggesting underdevelopment of immobile regions,

Fig. 7 Conceptual model of karst conduits
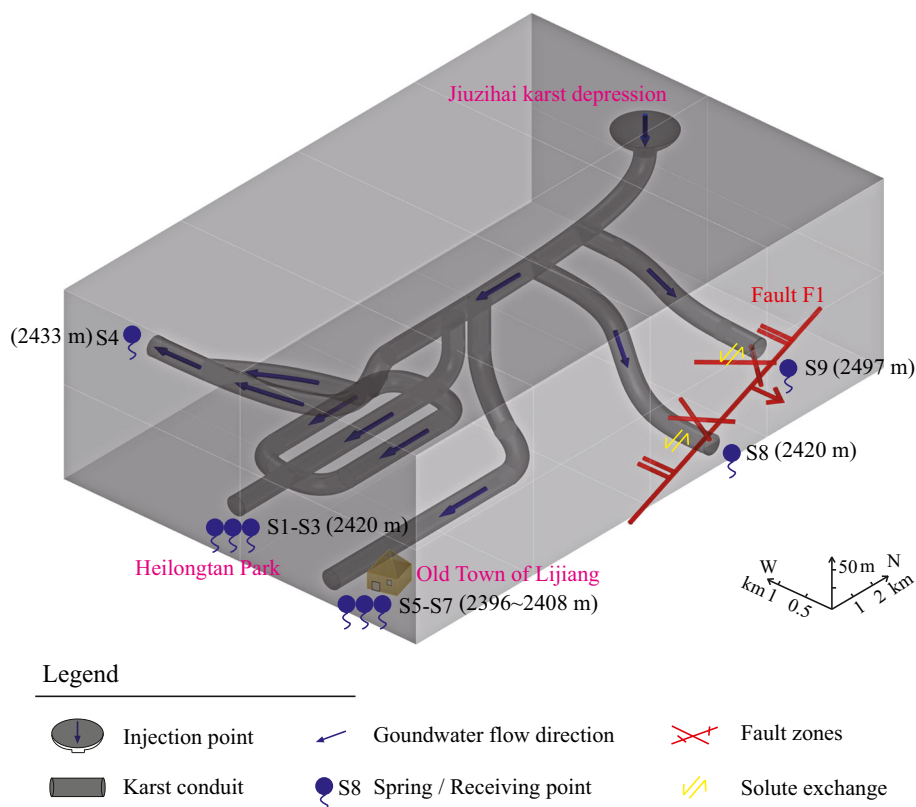
e.g., dead-end passages along the main flow channel. The average elevation of the OTLJ Springs is about 5 m lower than that of the groundwater level in the observation well according to the measurements from Mar. 1992 to Dec. 2011. Thus, it appears that approaching the springs, conduits are mostly below the level of the regional groundwater level and thus fully saturated. These fully saturated conduits are accounted for in that the outflow of S5–S7 only showed a decreasing trend during the dried-up periods for S1–S3. In the previous tracer test conducted in 2012 (Southwest Nonferrous Kunming Exploration Surveying and Designing (Institute) Inc., unpublished report, 2012), ammonium molybdate was used as a tracer and injected into the pool of HP to find out whether the S5 and S6 springs are supplied by the HP Springs. In that study, single-peaked BTCs were obtained, which confirms the hydraulic connection between OTLJ and HP. However, in this study, in contrast to S1–S3, higher concentrations and fewer peaks were obtained from curves received at S5–S7 (Fig. 4a–f and Fig. 5a–c). Thus, it can be deduced that regional groundwater is the predominant recharge source of the OTLJ Springs and streamflow seepage from HP only accounts for a very limited proportion.

Only one major flow path was determined from Jiuzihai karst depression to each spring located in the fault zones (S8 and S9; Fig. 7). In contrast to S5–S7, the 2RNE model delivered the lower partitioning coefficient (71–80%) and the higher mass transfer coefficient (0.48–1.23) for S8–S9,

indicating higher percentage of the immobile fluid region and more extensive exchange between mobile and immobile regions along the flow paths. In practical terms, fracture zones generated by tectonic activity provide favorable conditions for the emergence of immobile fluid regions. In addition, compared with S8, S9 produced significantly lower velocities, likely due to the lower permeability of the flow path.

Implications of tracer tests for the evaluation of an artificial recharge scheme

Tracer tests were firstly employed for the evaluation of an artificial recharge scheme in a karstic area. By injecting tracers into the recharge area of the scheme, it was possible to acquire more intuitionistic and realistic information related to the practical engineering. According to the tracer tests, Jiuzihai karst depression is confirmed to be the main concentrated recharge area of the whole karst aquifer system. This system is characterized by multiple conduits in which only the conduits connecting Jiuzihai with the springs in HP and OTLJ can be regarded as the available recharge pathways for this scheme. Highly conductive conduits and triple-conduit structures provide favorable conditions for the artificial recharge scheme. In 2018, a similar tracer experiment had been conducted in the study area. According to Han et al. (2019), 500 kg of potassium iodide powder were dissolved and injected into the sinkhole of Jiuzihai karst depression. Results show that this

depression is significantly connected with the springs in HP and OTLJ through deep-buried karst conduits. It was also confirmed by Han et al. (2019) that the dried-up situation can be effectively repaired by recharging in the depression.

Tracer tests also suggest that the shortest recharge time from Jiuzihai to HP Springs is about 190 h (t_{le}). Previous study concluded that the time of first tracer detection and maximum concentration (or peak time) yield an estimate of maximum flow velocity (v_{le}) and dominant velocity (v_{p1}), respectively (Goldscheider et al. 2008). Thus, it can be deduced that the discharge of HP Springs will increase after 220 h (t_{p1}) of the implementation of artificial recharge in Jiuzihai. Similarly, it will take about 300 h for OTLJ Springs to receive the recharge. Overall, time lags of the artificial concentrated recharge are 9.2 and 12.5 days for springs in HP and OTLJ respectively, while the time lag of natural recharge by regional precipitation is about 2–3 months according to Li (2016). This intensive and rapid recharging process forms one of the advantages of the scheme; however, it should be noticed that the tracers were forced into the aquifer with pressure by flushing water. This artificial pressure-bearing injection differs from the natural infiltration in practical engineering. Consequently, it will take a little more time in the implementation of the scheme to receive the recharged water.

Clear Spring and Fault Springs are identified as the leakages in this scheme. The pathway between Jiuzihai karst depression and Clear Spring characterize high permeability and exhibit two main branches of drainage. Owing to the shortest transporting distance, recharged water is predicted to be firstly received at the Fault Springs. Besides, as the main fault zones with considerable extension length, there might be other undiscovered leakages along the F1 due to the limitation of field investigation.

Since the fully dissolved and mixed tracers were injected into the aquifer and monitored in the same period under the condition of no precipitation, the tracer recoveries calculated at each spring can offer references for the distribution proportion of recharged water. Considering the possibility of interference with the recoveries obtained from Γ^- as discussed in section 'Tracer recoveries', only the recoveries from uranine are used for the following analysis. As shown in Fig. 8, tracer mass calculated at the HP Springs and OTLJ Springs accounts for 24 and 21% of the total recovered tracer mass, respectively, compared with 40 and 15% at Clear Spring and Fault Springs. This indicates that the springs to be recharged (HP Springs and OTLJ Springs) and the springs considered as leakages (Clear Spring and Fault Springs) respectively share 45 and 55% of the increased outflow provided by recharged water.

Conclusion

By conducting the multitracer tests, it was possible to determine the hydrogeological conditions from Jiuzihai karst depression to the water receiving springs, and therefore to provide references for the evaluation of an artificial recharge scheme. Interpretation and modeling of the BTCs provide insights into the transporting mechanisms of karst groundwater and the structural characteristics of the aquifer. The drainages between Jiuzihai karst depression and each spring are respectively characterized by a triple conduit (HP Springs), double conduit (Clear Spring) and single conduit (OTLJ Springs and Fault Springs). With higher flow velocities and multiple conduits, favorable recharge conditions can be recognized from the recharge area to HP springs. According to the temporal variation of tracer concentrations, it is predicted that the springs in HP and OTLJ will be effectively recharged by the water supplied at Jiuzihai karst depression after 9.2 and 12.5 days, respectively. By setting additional springs as receiving points during the tracer tests, it is possible to identify the leakages of the recharge scheme, which included Clear

Fig. 8 Proportional distribution of injected uranine

Distribution proportion of recovered uranine
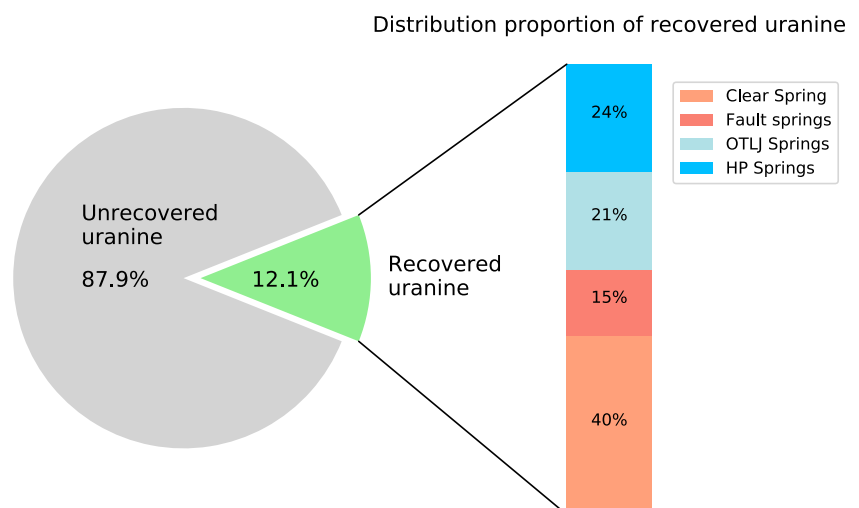
Spring and Fault Springs. Based on the calculation of the uranine recoveries, it can be further deduced that the springs to be recharged (HP Springs and OTLJ Springs) and the springs considered as leakages, respectively, share 45 and 55% of the increased outflow. Parameters and spatially resolved information obtained from tracer tests allow for a better understanding of the karst aquifer and karst groundwater and therefore may help to restore and preserve karst water resources in the Old Town of Lijiang. Moreover, this study broadens the possibility of applying combined tracer tests to practical engineering projects.

Declarations

Conflict of interest The authors declare that they have no conflict of interest.

References

Al-Assa'd TA, Abdulla FA (2010) Artificial groundwater recharge to a semi-arid basin: case study of Mujib aquifer, Jordan. Environ Earth Sci 60(4):845–859. https://doi.org/10.1007/s12665-009-0222-2

Barberá JA, Mudarra M, Andreo B, De 1TB (2017) Regional-scale analysis of karst underground flow deduced from tracing experiments: examples from carbonate aquifers in Malaga province, southern Spain. Hydrogeol J 26(3):1–18. https://doi.org/10.1007/s10040-017-1638-5

Brouyere S, Carabin G, Dassargues A (2005) Influence of injection conditions on field tracer experiments. Ground Water 43(3):389–400. https://doi.org/10.1111/j.1745-6584.2005.0041.x

Couture RA, Seitz MG (1983) Sorption of anions of iodine by iron oxides and kaolinite. Nucl Chem Waste Manag 4(4):301–306. https://doi.org/10.1016/0191-815X(83)90055-4

Daher W, Pistre S, Kneppers A, Bakalowicz M, Najem W (2011) Karst and artificial recharge: theoretical and practical problems: a preliminary approach to artificial recharge assessment. J Hydrol 408(3): 189–202. https://doi.org/10.1016/j.jhydrol.2011.07.017

Dar FA, Arora T, Warsi T, Devi AR, Wajihuddin M, Grutzamer G, Bodhankar N, Ahmed S (2017) 3-D hydrogeological model of limestone aquifer for managed aquifer recharge in Raipur of Central India. Carbonates Evaporites 32(4):459–471. https://doi.org/10.1007/s13146-016-0304-7

Dewaide L, Collon P, Poulain A, Rochez G, Hallet V (2018) Double-peaked breakthrough curves as a consequence of solute transport through underground lakes: a case study of the Furfooz karst system, Belgium. Hydrogeol J 26:641–650. https://doi.org/10.1007/s10040-017-1671-4

Field MS, Leij FJ (2012) Solute transport in solution conduits exhibiting multi-peaked breakthrough curves. J Hydrol 440–441:26–35. https://doi.org/10.1016/j.jhydrol.2012.03.018

Field MS, Nash SG (1997) Risk assessment methodology for karst aquifers: (1) estimating karst conduit-flow parameters. Environ Monit Assess 47(1):1–21. https://doi.org/10.1023/A:1005753919403

Field MS, Pinsky PF (2000) A two-region nonequilibrium model for solute transport in solution conduits in karstic aquifers. J Contam Hydrol 44(3–4):329–351. https://doi.org/10.1016/S0169-7722(00)00099-1

Geyer T, Birk S, Licha T, Liedl R, Sauter M (2007) Multitracer test approach to characterize reactive transport in karst aquifers. Ground Water 45(1):36–45. https://doi.org/10.1111/j.1745-6584.2006.00261.x

Goel AK, Kumar R (2005) Economic analysis of water harvesting in a mountainous watershed in India. Agric Water Manage 71(3):257–266. https://doi.org/10.1016/j.agwat.2004.09.005

Goeppert N, Goldscheider N (2019) Improved understanding of particle transport in karst groundwater using natural sediments as tracers. Water Res 166:115045. https://doi.org/10.1016/j.watres.2019.115045

Goldscheider N (2008) A new quantitative interpretation of the long-tail and plateau-like breakthrough curves from tracer tests in the artesian karst aquifer of Stuttgart, Germany. Hydrogeol J 16(7):1311–1317. https://doi.org/10.1007/s10040-008-0307-0

Goldscheider N, Meiman J, Pronk M, Smart C (2008) Tracer tests in karst hydrogeology and speleology. Int J Speleol 37(1):27–40. https://doi.org/10.5038/1827-806x.37.1.3

Goppert N, Goldscheider N (2008) Solute and colloid transport in karst conduits under low- and high-flow conditions. Ground Water 46(1):61–68. https://doi.org/10.1111/j.1745-6584.2007.00373.x

Han X, Chen X, Zheng KX, Liu S (2019) Application of the tracer test in karst hydrogeological prospecting: an example of Heilongtan, Lijiang, Yunnan (in Chinese with English abstract). Carsol Sin 38(4):524–531

Hao Y, Zhu Y, Zhao Y, Wang W, Du X, Yeh TCJ (2009) The role of climate and human influences in the dry-up of the Jinci Springs, China1. J Am Water Resour Assoc 45(5):1228–1237. https://doi.org/10.1111/j.1752-1688.2009.00356.x

Hartmann A, Goldscheider N, Wagener T, Lange J, Weiler M (2014) Karst water resources in a changing world: review of hydrological modeling approaches. Rev Geophys 52(3):218–242. https://doi.org/10.1002/2013rg000443

Hu QH, Moran JE (2005) Simultaneous analyses and applications of multiple fluorobenzoate and halide tracers in hydrologic studies. Hydrol Process 19(14):2671–2687. https://doi.org/10.1002/hyp.5780

Jiang C, Gao X, Hou B, Zhang S, Zhang J, Li C, Wang W (2020) Occurrence and environmental impact of coal mine goaf water in karst areas in China. J Clean Prod 275:123813. https://doi.org/10.1016/j.jclepro.2020.123813

Kang F, Jin M, Qin P (2011) Sustainable yield of a karst aquifer system: a case study of Jinan springs in northern China. Hydrogeol J 19(4):851–863. https://doi.org/10.1007/s10040-011-0725-2

Kang XB, Wang Y, Zhang H, Cao J (2013) Hydrogeologic features and influence factors of zero flow of the Heilongtan spring group in Lijiang (in Chinese with English abstract). Carsol Sin 32(4):398–403

Klaas DKSY, Imteaz MA, Sudiayem I, Klaas EME, Klaas ECM (2020) Assessing climate changes impacts on tropical karst catchment: implications on groundwater resource sustainability and management strategies. J Hydrol 582:124426. https://doi.org/10.1016/j.jhydrol.2019.124426

Knoll P, Scheytt T (2018) A tracer test to determine a hydraulic connection between the Lauchert and Danube karst catchments (Swabian

Alb, Germany). Hydrogeol J 26(2):429–437. https://doi.org/10.1007/s10040-017-1678-x

Kübeck C, Maloszewski PJ, Benischke R (2013) Determination of the conduit structure in a karst aquifer based on tracer data: Lurbach system, Austria. Hydrol Process 27(2):225–235. https://doi.org/10.1002/hyp.9221

Lauber U, Goldscheider N (2014) Use of artificial and natural tracers to assess groundwater transit-time distribution and flow systems in a high-alpine karst system (Wetterstein Mountains, Germany). Hydrogeol J 22(8):1807–1824. https://doi.org/10.1007/s10040-014-1173-6

Lauber U, Ufrecht W, Goldscheider N (2014) Spatially resolved information on karst conduit flow from in-cave dye-tracing. Hydrol Earth Syst Sci 18:435–445. https://doi.org/10.5194/hess-18-435-2014

Leibundgut C, Maloszewski P, Külls C (2009) Tracers in hydrology. Hydrol Wasserbewirtsch 53(6):418. https://doi.org/10.1002/9780470747148.fmatter

Li YX (2016) 基于时间序列分析的丽江黑龙潭泉域动态研究. [Dynamic research of the Lijiang Heilongtan spring system based on the time series analysis]. MSc Thesis, Chengdu University of Technology, China, pp 104

Li GQ, Field MS (2014) A mathematical model for simulating spring discharge and estimating sinkhole porosity in a karst watershed. Grundwasser 19(1):51–60. https://doi.org/10.1007/s00767-013-0243-3

Long AJ, Sawyer JF, Putnam LD (2008) Environmental tracers as indicators of karst conduits in groundwater in South Dakota, USA. Hydrogeol J 16(2):263–280. https://doi.org/10.1007/s10040-007-0232-7

Luhmann AJ, Covington MD, Alexander SC, Chai SY, Schwartz BF, Groten JT, Alexander EC (2012) Comparing conservative and non-conservative tracers in karst and using them to estimate flow path geometry. J Hydrol 448:201–211. https://doi.org/10.1016/j.jhydrol.2012.04.044

Luo Q, Yang Y, Qian J, Wang X, Chang X, Ma L, Li F, Wu J (2020) Spring protection and sustainable management of groundwater resources in a spring field. J Hydrol 582:124498. https://doi.org/10.1016/j.jhydrol.2019.124498

Maloszewski P, Zuber A (1992) On the calibration and validation of mathematical models for the interpretation of tracer experiments in groundwater. Adv Water Resour 15(1):47–62. https://doi.org/10.1016/0309-1708(92)90031-V

Małoszewski P, Wachniew P, Czupryński P (2006) Study of hydraulic parameters in heterogeneous gravel beds: constructed wetland in Nowa Słupia (Poland). J Hydrol 331(3–4):630–642. https://doi.org/10.1016/j.jhydrol.2006.06.014

Morales T, de Valderrama IF, Uriarte JA, Antiguedad I, Olazar M (2007) Predicting travel times and transport characterization in karst conduits by analyzing tracer-breakthrough curves. J Hydrol 334(1–2):183–198. https://doi.org/10.1016/j.jhydrol.2006.10.006

Nerantzaki SD, Nikolaidis NP (2020) The response of three Mediterranean karst springs to drought and the impact of climate change. J Hydrol 591:125296. https://doi.org/10.1016/j.jhydrol.2020.125296

Oehlmann S, Geyer T, Licha T, Sauter M (2015) Reducing the ambiguity of karst aquifer models by pattern matching of flow and transport on catchment scale. Hydrol Earth Syst Sci 19(2):893–912. https://doi.org/10.5194/hess-19-893-2015

Ostad-Ali-Askari K, Shayannejad M, Ghorbanizadeh-Kharazi H (2017) Artificial neural network for modeling nitrate pollution of groundwater in marginal area of Zayandeh-Rood River, Isfahan, Iran. KSCE J Civ Eng 21(1):134–140. https://doi.org/10.1007/s12205-016-0572-8

Ostad-Ali-Askari K, Ghorbanizadeh Kharazi H, Shayannejad M, Zareian MJ (2019) Effect of management strategies on reducing negative impacts of climate change on water resources of the Isfahan–Borkhar aquifer using MODFLOW. River Res Appl 35(6):611–631. https://doi.org/10.1002/rra.3463

Ostad-Ali-Askari K, Kharazi HG, Shayannejad M, Zareian MJ (2020) Effect of climate change on precipitation patterns in an arid region using GCM models: case study of Isfahan-Borkhar plain. Nat Hazards Rev 21(2):04020006. https://doi.org/10.1061/(ASCE)NH.1527-6996.0000367

Perrin J, Luetscher M (2008) Inference of the structure of karst conduits using quantitative tracer tests and geological information: example of the Swiss Jura. Hydrogeol J 16(5):951–967. https://doi.org/10.1007/s10040-008-0281-6

Pronk M, Goldscheider N, Zopfi J (2007) Particle-size distribution as indicator for fecal bacteria contamination of drinking water from karst springs. Environ Sci Technol 41(24):8400–8405. https://doi.org/10.1021/es071976f

Pronk M, Goldscheider N, Zopfi J, Zwahlen F (2009) Percolation and particle transport in the unsaturated zone of a karst aquifer. Ground Water 47(3):361–369. https://doi.org/10.1111/j.1745-6584.2008.00509.x

Pu T, He YQ, Zhang T, Wu JK, Zhu GF, Chang L (2013) Isotopic and geochemical evolution of ground and river waters in a karst dominated geological setting: a case study from Lijiang basin, South-Asia monsoon region. Appl Geochem 33:199–212. https://doi.org/10.1016/j.apgeochem.2013.02.013

Qi JH, Xu M, Cen XY, Wang L, Zhang Q (2018) Characterization of karst conduit network using long-distance tracer test in Lijiang, Southwestern China. Water 10(7):949. https://doi.org/10.3390/w10070949

Schilling OS, Cook PG, Brunner P (2019) Beyond classical observations in hydrogeology: the advantages of including exchange flux, temperature, tracer concentration, residence time, and soil moisture observations in groundwater model calibration. Rev Geophys 57(1):146–182. https://doi.org/10.1029/2018RG000619

Schrader A, Winde F, Erasmus E (2014) Using impacts of deep-level mining to research karst hydrology: a Darcy-based approach to predict the future of dried-up dolomitic springs in the Far West Rand Goldfield (South Africa), part 2—predicting inter-compartmental flow and final groundwater tables. Environ Earth Sci 72(7):2583–2595. https://doi.org/10.1007/s12665-014-3298-2

Sivelle V, Jourde H, Bittner D, Mazzilli N, Tramblay Y (2021) Assessment of the relative impacts of climate changes and anthropogenic forcing on spring discharge of a Mediterranean karst system. J Hydrol 598:126396. https://doi.org/10.1016/j.jhydrol.2021.126396

Stevanović Z (2015) Damming underground flow to enhance recharge of karst aquifers in the arid and semi-arid worlds. Environ Earth Sci 75(1):35. https://doi.org/10.1007/s12665-015-5086-z

Sun YH, Liu NN, Shang JX, Zhang JY (2017) Sustainable utilization of water resources in China: a system dynamics model. J Clean Prod 142:613–625. https://doi.org/10.1016/j.jclepro.2016.07.110

Toride N, Leij FJ, Van Genuchten MT (1995) The CXTFIT code for estimating transport parameters from laboratory or field tracer experiments. Version 2.0, US Salinity Laboratory, Riverside, CA

Tóth J (1963) A theoretical analysis of groundwater flow in small drainage basins. J Geophys Res 68(16):4795–4812. https://doi.org/10.1029/JZ068i016p04795

van Genuchten MT, Šimůnek J, Leij FJ, Toride N, Šejna M (2012) STANMOD: model use, calibration, and validation. Am Soc Agric Biol Eng 55(4):1353–1366

Xanke J, Jourde H, Liesch T, Goldscheider N (2016) Numerical long-term assessment of managed aquifer recharge from a reservoir into a karst aquifer in Jordan. J Hydrol 540:603–614. https://doi.org/10.1016/j.jhydrol.2016.06.058

Yin BL, Guan DJ, Zhou LL, Zhou J, He XJ (2020) Sensitivity assessment and simulation of water resource security in karst areas within the

context of hydroclimate change. J Clean Prod 258:120994 https://doi.org/10.1016/j.jclepro.2020.120994

Yoshida S, Uchida YM (1992) Studies on the sorption of I− (iodide) and IO3− (iodate) onto andosols. Water Air Soil Pollut 63:321–329. https://doi.org/10.1007/BF00475499

Zeng C, Yang R, Yang MM, Hu JC, Fan YH (2013) Artificial neural network simulation to zero flow of the Heilongtan spring groups in Lijiang (in Chinese with English abstract). Carsol Sin 32(4):391–397

Zeng C, Liu Z, Yang J, Yang R (2015) A groundwater conceptual model and karst-related carbon sink for a glacierized alpine karst aquifer, southwestern China. J Hydrol 529:120–133. https://doi.org/10.1016/j.jhydrol.2015.07.027

Zhang Z, Wang W (2021) Managing aquifer recharge with multi-source water to realize sustainable management of groundwater resources in Jinan, China. Environ Sci Pollut Res 28(9):10872–10888. https://doi.org/10.1007/s11356-020-11353-3

Publisher's note Springer Nature remains neutral with regard to jurisdictional claims in published maps and institutional affiliations.